http://doi.org/10.24867/JPE-2020-01-015

Journal of Production Engineering

Vol.23 No.1

JPE (2020) Vol.23 (1) Original Scientific Paper

Gupta, V., Mehra V., Khanna, P.

MATHEMATICAL MODELLING TO PREDICT BEAD GEOMETRY AND SHAPE RELATIONSHIPS IN MIG WELDING OF STAINLESS STEEL 202

Received: 06 March 2020 / Accepted: 18 June 2020

Abstract: *In the current investigative work, mathematical models have been established to predict the weld bead geometry and shape relationships in Metal Inert Gas welding for 6mm plates of SS 202 grade. The filler metal used is a continuously fed solid metal wire of stainless steel 304L with argon gas serving the purpose of shielding the weld pool from the atmosphere. To obtain experimental samples, the design matrix was developed using the statistical technique of central composite rotatable design (CCRD). Analysis of Variance (ANOVA) technique was used for the adequacy check of the models developed. The models developed can be used to find direct and interaction effect of the input parameters, namely welding speed (WS), voltage (V), nozzle to plate distance (NPD), torch angle (Θ) and wire feed rate (WFR) on the weld bead geometry (reinforcement height (H), depth of penetration (P) and bead width (W)); and on the shape relationships such as WPSF (weld penetration shape factor), WRFF (weld reinforcement form factor) and dilution.*

Key words: *Stainless Steel Grade 202, MIG Welding, Central Composite Rotatable Design, Mathematical Model, ANOVA, Response Surface Methodology, F-ratio ANOVA*

Matematičko modeliranje za predviđanje geometrije nanošenja zavara i funkcija oblika vara pri MIG zavarivanju nerđajućeg čelika 202. *U predtavljenom istraživačkom radu uspostavljeni su matematički modeli koji predvidjaju geometriju nanesenog zavara i funkciju oblika pri zavarivanju metalnim inertnim gasom ploče debljine 6 mm nerdjajućeg čelika 202. Korišćeni metal za punjenje je neprekidna metalna žica od nehrđajućeg čelika 304L sa argonskim gasom koji služi za zaštitu zone zavarivanja od atmosfere. Da bi se dobili eksperimentalni uzorci, dizajnirana je matrica dizajna koristeći statističku tehniku centralnog kompozitnog dizajna eksperimenta (CCRD). Za ispitivanje adekvatnosti razvijenih modela korišćena je analiza varijance (ANOVA). Razvijeni modeli se mogu koristiti za pronalaženje direktnog i interaktivnog uticaja ulaznih parametara, a to su brzina zavarivanja (WS), napon (V), udaljenost između mlaznice i ploče (NPD), ugao gorionika (Θ) i brzina dotoka žice (WFR) na geometriju nanesenog zavara (visina armature (H), dubina prodora (P) i širina zrna (W)); i na funkciju oblika vara kao što su WPSF (faktor oblika prodora zavarivanja), VRFF (faktor oblika armature za zavarivanje) i razblaživanje.*

Ključne reči: *Nerđajući čelik 202, MIG zavarivanje, centralni kompozicioni dizajn eksperimenta, matematički model, ANOVA, metodologija odzivne površine, F-odnos ANOVA.*

1. INTRODUCTION

Stainless Steel 202 is an austenitic grade steel which is finding extensive use in fabrication industry as well as household applications, owing to being cost effective while still retaining the mechanical properties and corrosion resistance to other austenitic grade steels. Nitrogen addition results in approximately 50% higher yield strength than 300 series austenitic steels. They are weldable by all processes. Its exceptional resistance to corrosion even in adverse environments makes it suitable for the manufacturing of various industrial products like automotive fuel tanks, catalytic convertors and turbochargers, chassis for vehicles, architectural panelling, railings, structural components etc. [1]. The composition of the steel and its mechanical properties are represented in Table 1 and 2 respectively.

The need of welding for any manufacturing industry cannot be emphasized enough. With the help of metal inert gas welding, it has become a lot easier to weld stainless steel and that too rapidly [2]. In general, the dimensions of weld bead determine the quality and performance of a weld joint [3]. Therefore, it is essential to make sure that for any joint, the weld bead size is according to what the loading conditions demand at that particular joint. For different loading conditions; be it static, impact or fluctuating, an appropriate weld bead size can be calculated from a stress analysis at the joint [5]. Once an appropriate weld bead size is calculated, it is required to find out the best combination of input parameters which will achieve the desired geometry. For doing so, equations giving output parameters as a function of input parameters is required. But, with so many interacting input parameters, it is extremely difficult to develop an analytical model for the same.
So, instead, mathematical models are developed and fed into the system to make the robotic welding equipment more efficient [4].

Katherasan et al (2013) discussed the effect of various combinations of Argon and CO2 gas combinations as shielding gases for MIG welding [6]. In the present setup, 100% argon gas has been used for shielding purpose, since it doesn't dissociate at high temperatures, thereby preventing any turbulence in the welding arc; and being an inert gas, does not react with the weld pool metals and deteriorating the quality of the weld.

In the current work, CCRD technique was used to develop the design matrix for conducting the experiment. ANOVA technique has been used to check the adequacy of the equations developed [4]. The weld bead dimensions are shown in Figure 1.

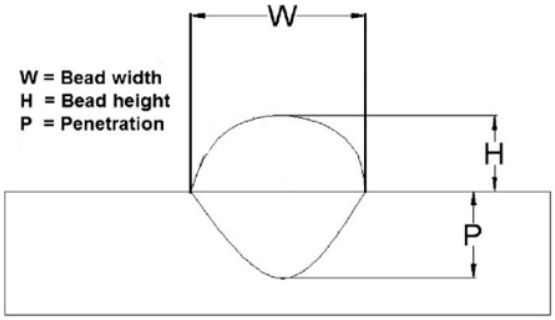

Fig. 1. Weld Bead Geometry [7]

2. EXPERIMENTAL SETUP

The experimental setup used in the present investigative work consists of a MIG welding power source, rectifier type with open circuit voltage of 45 Volts and rated current capacity of 400 amperes, 100% duty cycle and flat V-I Characteristics. 100% argon gas is used for shielding and the flow rate is maintained at about 15 liters/ min throughout the experiment. To maintain the desired welding speed and ensure reproducibility of results, a mechanized welding unit is used which provides a step-less control of carriage speed from 0 to 50 cm/min. A variable frequency drive has been used to control the speed of carriage motor. The complete setup is shown in Figure 2.


Fig. 2. Experimental Setap

Element	C	Mn	S	P	Si	Ni	Cr	N	Cu
Percentage (%)	0.11	10.09	.007	0.053	0.042	0.44	14.24	0.162	0.51

Table 1. Chemical Composition

Grade	Mechanical Properties	Ultimate Tensile Strength (MPa)	Yield Strength (MPa)	% Elongation	Hardness (HRB)
202	ASTM A240	≥620	≥260	≥40	≤241

Table 2. Mechanical Properties

3. PLAN OF INVESTIGATION

The research work was carried out in the following steps:

1. Identification of input parameters and determining their working limits.
2. Development of design matrix.
3. Conducting experiments as per the design matrix and recording the observations.
4. Development of mathematical model.
5. Checking the significance of developed models.
6. Interpretation of results.

3.1 Identification of input parameters and determining their working limits

From an extensive literature survey and preliminary experimentations, the following input parameters of WS, WFR, θ, V and NPD were found to have a significant effect on bead geometry and shape relationships. Trial runs were conducted by changing the numerical values of one of the five input parameters, while keeping the other four as constant, for determining the working limits. The working limits were fixed by observing the weldments for the following-

- No spatters on the weldments
- No visible signs of porosity
- No visible cracks, undercut or burn-through

3.2 Development of Design Matrix

As shown in table-3, CCRD technique was used to develop the design matrix which resulted in 32 experimental runs, consisting of five input parameters, each at different five levels Lower limits are coded as -2 and upper limits are coded as +2.

Welding Variables	Units	Abbreviations	Limits				
			-2	-1	0	1	2
Wire Feed Rate	m/mins	WFR	0.3	0.6	0.9	1.2	1.5
Welding Speed	cm/mins	WS	30	35	40	45	50
Arc Voltage	volts	V	14	16	18	20	22
Nozzle to plate distance	mm	NPD	10.0	12.5	15.0	17.5	20.0
Electrode to work angle	degrees	Θ	70 °	80 °	90 °	100 °	110 °

Table 3. Welding variables and their limits

3.3 Conducting the experiment and recording the observations

32 welding runs were performed on standard specimens in the order shown in the matrix below. This sequence of experimental runs will reduce machine systematic error.

3.4 Development of mathematical model

The output response parameters can be related to input parameters in form of equations as:

$x = f(A, B, C, D, E)$

where 'x' is a response parameter and A - Wire feed rate, B - Welding speed, C- Voltage, D- Nozzle to plate distance, E- Torch Angle

A generalised form of mathematical equation is written in a form as shown below, which relates input parameters to output responses:

$x = \beta o + \beta 1a + \beta 2b + \beta 3c + \beta 3d + \beta 3e + \beta 12ab + \beta 13ac + \beta 14ad + \beta 15ae + \beta 23bc + \beta 24bd + \beta 25be + \beta 34cd + \beta 35ce + \beta 45de + \beta 11a2 + \beta 22b2 + \beta 33c2 + \beta 44d2 + \beta 55e2$

where $\beta 1$, $\beta 2$, $\beta 11$, $\beta 12$ …… are regression coefficients.

	Run	Wire Feed Rate	Welding Speed	Voltage	Nozzle To Plate Distance	Torch Angle	Depth Of Penetration	Height	Width	WPSF	WRFF	DILUTION
		m/min	cm/min	Volts	mm	degree	mm	mm	mm			
4	1	1.2	45	16	12.5	100	4.72	8.29	1.56	1.34	4.63	83.18
11	2	0.6	45	16	17.5	100	2.48	4.86	1.62	1.56	4.82	51.26
32	3	0.9	40	18	15	90	4.44	8.39	1.33	2.25	6.29	73.12
27	4	0.9	40	18	15	90	3.86	9.93	1.69	2.57	6.41	68.85
9	5	0.6	35	16	17.5	80	3.27	6.36	1.76	1.94	5.44	53.24
12	6	1.2	45	16	17.5	80	4.36	7.43	1.88	2.16	7.26	57.49
2	7	1.2	35	16	12.5	80	6.00	8.19	1.50	1.36	8.16	76.9
14	8	1.2	35	20	17.5	80	5.98	9.14	1.11	1.38	12.09	87.53
26	9	0.9	40	18	15	110	3.58	8.51	1.29	2.37	5.62	65.28
29	10	0.9	40	18	15	90	3.68	8.48	1.35	2.29	6.26	68.17
15	11	0.6	45	20	17.5	80	3.01	8.05	0.60	2.67	13.37	74.77
13	12	0.6	35	20	17.5	100	3.28	6.46	1.27	1.97	8.90	54.33
21	13	0.9	40	14	15	90	3.34	7.74	1.76	2.32	1.97	54.07
8	14	1.2	45	20	12.5	80	5.78	9.84	0.76	1.70	11.91	84.72
19	15	0.9	30	18	15	90	4.64	10.79	1.37	2.04	7.89	62.5
20	16	0.9	50	18	15	90	3.07	6.86	1.31	2.23	8.43	69.56
18	17	1.5	40	18	15	90	6.53	9.99	1.62	1.24	9.07	84.44
5	18	0.6	35	20	12.5	80	4.69	7.81	0.44	1.07	10.45	87.07
30	19	0.9	40	18	15	90	4.00	8.93	1.459	2.23	6.12	68.78
24	20	0.9	40	18	20	90	4.05	7.80	1.46	1.78	8.86	55.59
28	21	0.9	40	18	15	90	4.00	8.93	1.46	2.23	6.12	68.78
17	22	0.3	40	18	15	90	2.79	7.26	1.14	1.95	6.23	77.27
7	23	0.6	45	20	12.5	100	3.85	5.21	0.65	1.64	7.93	81.51
3	24	0.6	45	16	12.5	80	3.62	4.89	0.98	1.35	4.74	72.62
6	25	1.2	35	20	12.5	100	5.56	9.89	1.56	1.78	9.46	71.66
23	26	0.9	40	18	10	90	5.03	7.88	1.08	1.46	6.53	75.62
1	27	0.6	35	16	12.5	100	3.76	7.73	1.51	2.06	2.81	61.55
16	28	1.2	45	20	17.5	100	6.27	9.34	0.58	1.48	10.72	85.85
22	29	0.9	40	22	15	90	5.56	9.13	1.01	1.99	11.98	78.44
25	30	0.9	40	18	15	70	4.79	7.13	1.33	1.33	10.52	76.31
31	31	0.9	40	18	15	90	4.00	8.93	1.46	2.23	6.12	68.78
10	32	1.2	35	16	17.5	100	4.42	8.71	1.99	2.84	4.56	42.64

Table 4. Response values for given values of input parameters

After putting the values of the measured output responses in the matrix, the design expert software gives the following equations:

Depth of penetration = 4 + 0.941A – 0.2499B + 0.4261C -0.2861D -0.2006E + 0.0764AB + 0.1503AC + 0.1781AD + 0.0051AE + 0.1048BC + 0.0766BD + 0.2181BE + 0.1399CD + 0.0857CE + 0.1267DE + 0.1672A2 – 0.0330B2 + 0.1157C2 + 0.1373D2 + 0.0508E2

Width = 9.03 + 1.04A – 0.5936B + 0.4997C – 0.0692D + 0.0650E + 0.2703AB + 0.1199AC – 0.1061AD + 0.2798AE + 0.2916BC + 0.2751BD – 0.2366BE + 0.123CD – 0.4174CE – 0.1264DE – 0.1691A2 – 0.1197B2 – 0.2199C2 – 0.3660D2 – 0.3717E2

Height of reinforcement = 1.47 + 0.1307A – 0.1106B – 0.3031C + 0.1111D + 0.0699E – 0.0115AB – 0.0060AC – 0.0977AD – 0.0565AE – 0.0626BC – 0.0211BD – 0.0779BE – 0.1014CD + 0.0329CE –

0.0969DE – 0.0329A2 – 0.0430B2 – 0.0318C2 – 0.0605D2 – 0.0510E2

WPSF = 2.30 – 0.0673A – 0.0045B – 0.0652C + 0.1816D + 0.1298E -0.0537AB – 0.1127AC – 0.0219AD + 0.0406AE + 0.1935BC – 0.0009BD – 0.2964BE – 0.0679CD – 0.0583CE – 0.1012DE – 0.1762A2 – 0.0402B2 – 0.0353C2 – 0.1703D2 – 0.1105E2

WRFF = 6.24 + 0.6666A + 0.1909 + 2.60C + 0.4886D - 1.23E – 0.1872AB – 0.2039AC –0.3823AD – 0.0316AE + 0.1590BC + 0.4273BD + 0.0767BE + 0.2241CD – 0.1265CE + 0.0821DE + 0.3333A2 + 0.4621B2 + 0.1658C2 + 0.3456D2 + 0.4394E2

Dilution = 69.35 + 2.83A + 2.94B + 7.39 C – 6.34D – 3.52E + 0.5337AB + 0.6587AC + 1.64AD + 0.9837AE – 0.2475BC + 0.4237BD + 5.42BE + 4.20CD - 1.20CE – 0.9713DE + 2.93A2 – 0.7798B2 – 0.7235C2 – 0.8860D2 + 0.4115E2

3.5 Adequacy check of model

ANOVA analysis of the mathematical models developed shows for every response parameter, the model to be significant and the lack of fit to be not significant. This is also evident by high values of R2 as shown in the tables. Also, the scatter diagrams between the predicted values and the actual results substantiate the result.

BEAD PARAMETER	FIRST ORDER TERMS		SECOND ORDER TERMS		LACK OF FIT		ERROR TERMS		F- RATIO	R^2	ADJUSTED R^2	ADEQUACY OF MODELS
	SS	df	SS	df	SS	df	SS	df				
PENETRA-TION	30.036	5	4.5531	15	0.5906	6	0.3155	5	20.87	0.9743	0.9276	Adequate
HEIGHT	3.3172	5	1.0053	15	0.3788	6	0.008	5	5.10	0.9027	0.7259	Adequate
WIDTH	40.6565	5	20.2447	15	0.9572	6	0.3016	5	4.46	0.8901	0.6904	Adequate
WPSF	1.407	5	4.7865	15	0.5016	6	0.0878	5	5.43	0.9081	0.7409	Adequate
WRFF	215.8244	5	27.6551	15	0.3613	6	0.0698	5	305.14	0.9982	0.9949	Adequate
DILUTION	2971.56	5	1176.28	15	78.51	6	16.81	5	24.09	0.9777	0.9371	Adequate

Table 5. ANOVA table to check adequacy of models

3.6 Interpretation of results

The graphical exhibition of the results obtained in the current investigative work, is shown in Fig. 3 to 7. The interpretation of these results is divided into two categories namely; direct effects and interaction effects with their explanation as follows:

3.6.1 Direct effect of WFR

In a constant voltage setup, as the WRF increases, more material melts so that the length of arc is constant. For more material to melt, the heat given to the weld pool increases. Since additional filler wire melts, the depth of penetration increases. As more filler material is deposited, the reinforcement height also increased and the material spreads on the joint, increasing the width of the bead.

As WFR rises, it is seen that the WPSF rises too, probably because percentage growth in width is more compared to the percentage growth in penetration. Similarly, WRFF decreases a bit probably because percentage rise in width is smaller than percentage rise in height. Due to increased current, more base plate is melted compared to the wire, thereby increasing the penetration and thus increasing dilution.

3.6.2 Direct effect of torch angle

As observed, the penetration declines with rise in torch angle, because as angle increases, the force by the welding arc gets directed in front of the weld pool, thereby reducing force towards the penetration. Height of reinforcement intensifies only slightly at the expense of penetration.

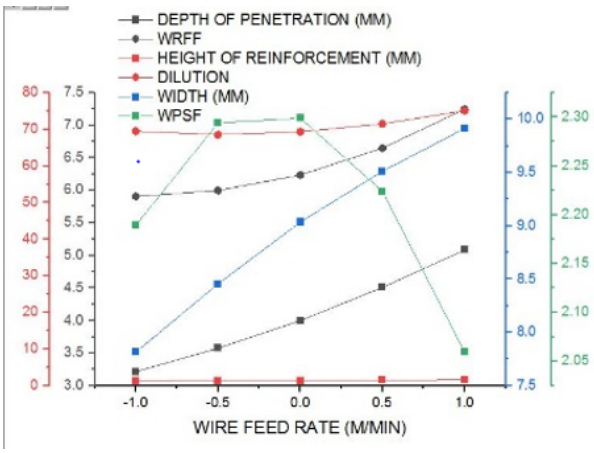

Fig. 3. Effect of WFR on Bead Geometry

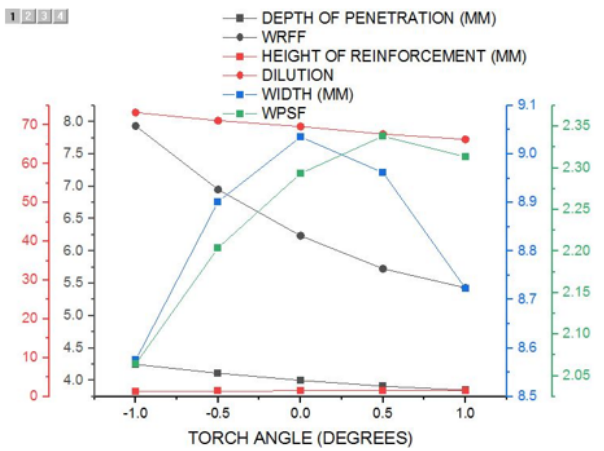

Fig. 4. Effect of Torch Angle on Bead Geometry

With an increase in the torch angle, dilution is observed to reduce as reduction in penetration area is more in comparison to reinforcement area. WRFF decreases due to percentage increase in height being more than the percentage increase in width. With the increase in torch angle, WPSF increases due to rise in width and decline in penetration.

3.6.3 Direct effect of NPD

As the NPD increases, length of unmelted wire between the nozzle tip and the arc increases, since the arc length remains constant (due to constant voltage). This causes more resistance to the path of current, thereby generating more heat between the nozzle and arc. So, before the wire even enters the arc, it is already very hot, which makes more of it to melt, thereby getting collected on top of the base plate, causing a rise in reinforcement. WPSF increases as NPD rises due to percentage decrease in penetration being greater than the percentage decrease in width. WRFF increases as NPD rises due to percentage increase in height being even less than the percentage decrease in the width of the bead. Dilution decreases since increasing NPD diverts more heat towards melting and depositing the molten metal and reduces the melting of parent plate.

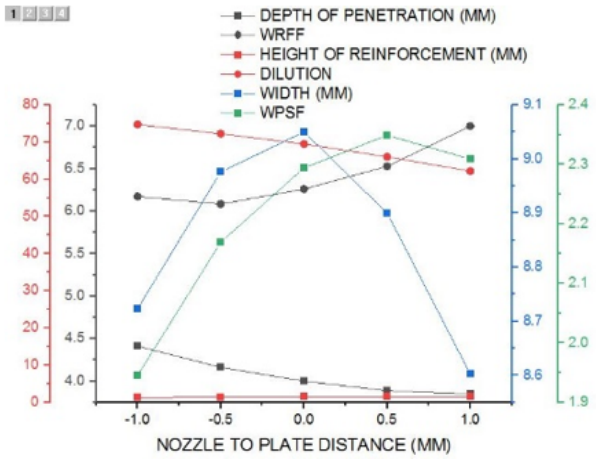

Fig. 5. Effect of NPD on Bead Geometry

3.6.4 Direct effect of voltage

As voltage increases, the depth of penetration and the bead width increase.

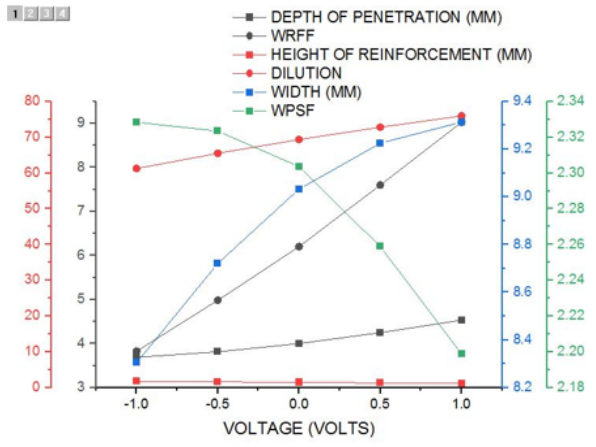

Fig. 6. Effect of Voltage on Bead Geometry

This can be explained from the fact that when voltage increases, a higher amount of heat is there at the wire side, which leads to more filler wire melting and hence increases deposition rate which in turn increases the penetration depth. Similarly, width of the bead becomes greater as the voltage intensifies, but at the expense of a slight decrease in reinforcement height. With rise in the voltage, the WRFF increase as the percentage decrease in the reinforcement height is more than percentage increase in the bead width. Also, the WPSF decreases probably because the percentage decrease in the penetration is slightly less than the decrease in the width percentage. Due to increased heat input, more base plate melted compared to the material deposited, thereby increasing dilution.

3.6.5 Direct effect of WS

As the WS becomes higher, less time is available for the filler wire to melt and thus deposit on the joint. As a consequence, the width, reinforcement height and the depth of penetration decreases.

WPSF remains nearly constant as the WRF rises as the percentage reduction in the penetration is nearly equal to percentage decrease in the bead width. But the WRFF rises with the rise in WFR as the percentage reduction in height is even less than the percentage in the bead width. As welding speed increased, an increase in the dilution was observed. This occurred because the percentage increase for melting of the parent metal was more, leading to rise in penetration area than the area of metal deposited.

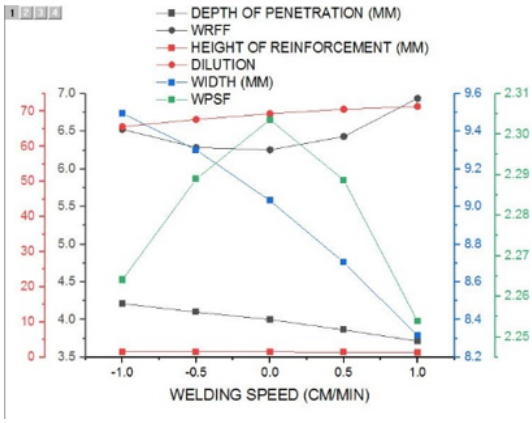

Fig. 7. Effect of Welding Speed on Bead Geometry

3.6.6 Interaction effect of WS and WFR on depth of penetration

It is evident that WFR has a positive effect on the depth of penetration. This is because, as the wire feed rate increases, more wire melts to keep a constant arc length. As more wire melts, more molten metal gets deposited between the plates, thereby increasing penetration. Also, the penetration reduces with increase in WS. This can be explained as the increased WS leads to a decrease in energy input, making the parent metal melt less and consequent less penetration. The maximum penetration depth of 5.23 mm is obtained at maximum WS and minimum WFR, whereas minimum depth of penetration of 2.88 mm is obtained at maximum WFR and minimum WS.

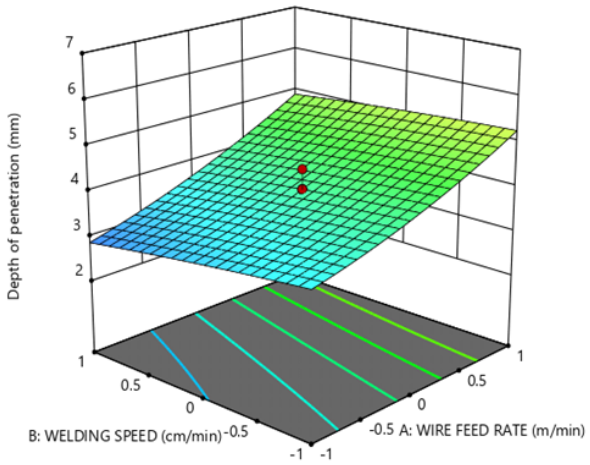

Fig. 8. Interaction effect of welding speed and WFR on Depth of penetration

3.6.7 Interaction effect of torch angle and NPD on height of reinforcement

It can be seen that NPD has a positive effect on the height of reinforcement. This could be because of increased length of unmelted wire entering the arc with the increase of NPD. This increase in wire length results in more resistive heating causing more melting of wire rather than the base metal thereby increasing the pile of molten filler on the base metal, increasing the height of reinforcement. At the same time, it can be seen that the height of reinforcement decreased with the increase in torch angle. It is due to the fact that as torch angle increase, the forward spread of the arc also increases, making the weld pool more shallow than deep. The maximum height of reinforcement of 1.50 mm is obtained at maximum NPD and minimum torch angle, whereas minimum depth of penetration of 1.08 mm is obtained at minimum NPD and torch angle.

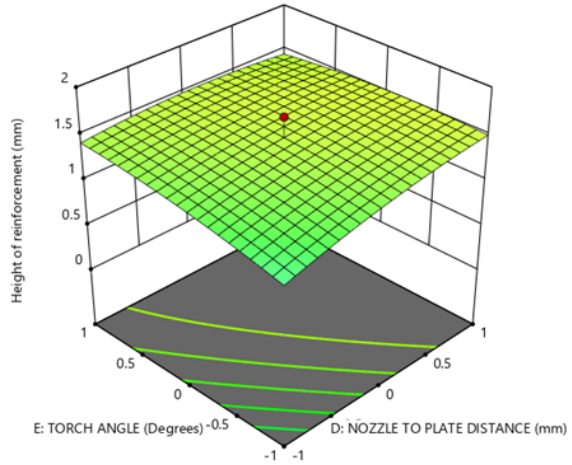

Fig. 9. Interaction effect of Torch angle and NPD on Height of reinforcement

3.6.8 Interaction effect of torch angle and WFR on width

It can be seen that as the WFR rises, the width of the bead rises as well. In order to maintain the arc length when the wire feed rate increases, more wire melts to increases the bead width. Also, the width rises as the torch angle increases. This can be understood that as the arc force is directed more ahead of the weld pool with increase in torch angle, which spreads the bead more increasing the bead width. The maximum depth of width of 9.87 mm is obtained at maximum wire feed rate and minimum, whereas minimum depth of penetration of 7.25 mm is obtained at maximum torch angle distance and minimum WFR.

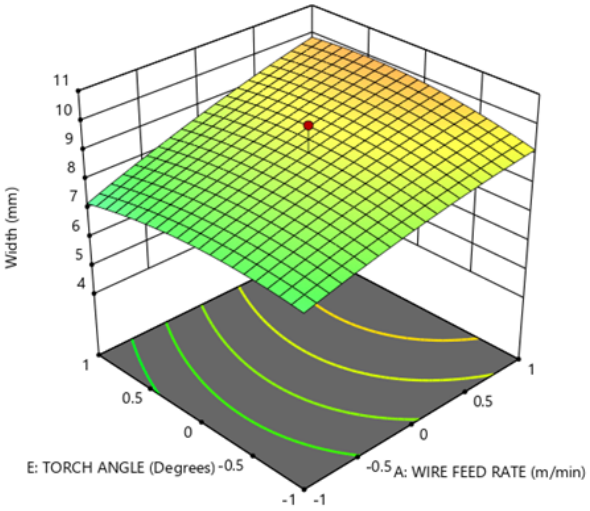

Fig. 10. Interaction effect of Torch angle and WFR on Width

3.6.9 Interaction effect of voltage NPD on depth of penetration

It can be seen that NPD a negative effect on the depth of penetration. This is because, with rise in NPD, the length of unmelted wire increase, and more energy which was supposed to go into melting the base metal is consumed in resistive heating of the unmelted wire. This leads to less melting of the base metal, and more piling up of the molten wire, eventually decreasing the depth of penetration. Also, as the voltage rises, energy input increases, making the parent plate melt more and consequently increase the penetration of the molten metal. The maximum depth of penetration of 4.81mm is obtained at maximum voltage and minimum NPD, whereas minimum depth of penetration of 3.40mm is obtained at maximum NPD and minimum voltage.

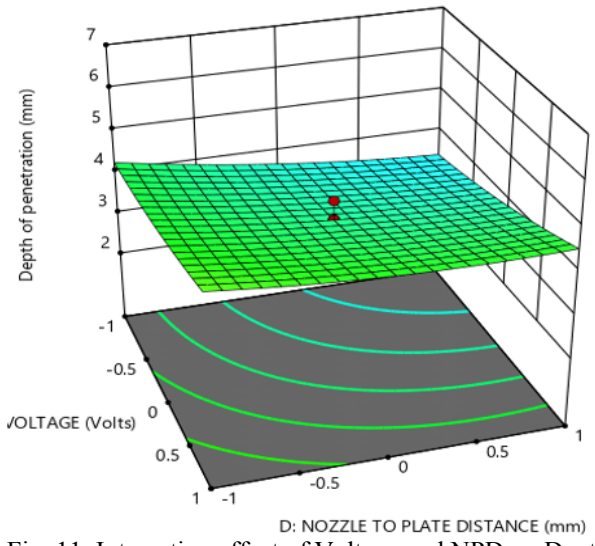

Fig. 11. Interaction effect of Voltage and NPD on Depth of penetration

4. CONCLUSION

1. For the development of mathematical models to predicting the weld bead dimensions, the technique of CCRD is found to be a useful and satisfactory tool.
2. Increasing the voltage has led to an increase in depth of penetration, width, dilution and WRFF but has decreased reinforcement height and WPSF.
3. An increase of welding speed has led to an increase of WRFF and dilution but a decrease in depth of penetration, width, and reinforcement height is observed with WPSF remaining nearly constant.
4. Increase in torch angle has led to an increase in width, reinforcement height and WPSF but with a decrease of penetration depth, WRFF and dilution.
5. Increase in the wire feed rate has led to an increment in depth of penetration, width, reinforcement height dilution and WRFF values but WPSF has decreased.
6. Increasing the nozzle to plate distance has resulted in increase of reinforcement height and WRFF but has decreased width, depth of penetration, dilution and WPSF.
7. The maximum depth of penetration of 5.23mm is obtained at maximum welding speed and minimum wire feed rate, whereas minimum depth of penetration of 2.88mm is obtained at maximum wire feed rate and minimum welding speed.
8. The maximum depth of width of 9.87mm is obtained at maximum wire feed rate and minimum, whereas minimum depth of penetration of 7.25mm is obtained at maximum torch angle distance and minimum wire feed rate.
9. The maximum height of reinforcement of 1.75mm is obtained at minimum voltage and welding speed, whereas minimum depth of penetration of 0.92mm is obtained at maximum voltage and welding speed.
10. No defects were found in any of the weldments.

5. REFERENCES

[1] Kalpakjian, S, "Manufacturing Engineering and Technology", Pearson Publication, 2018

[2] Parmar, R. S., "Welding Processes and Technology". Khanna Publishers, 10th edition, New Delhi, 2010

[3] Kolahan, F. and Heidari, M., "A New Approach for Predicting and Optimizing Weld Bead geometry in GMAW". International Journal of Aerospace and Mechanical Engineering, Vol.5, No.2, pp. 138-142, 2011

[4] Murugan, N., and Gunaraj, V. Prediction and control of weld bead geometry and shape relationships in submerged arc welding of pipes. Journal of material Processing Technology, 168(2005), pp478-484

[5] Budynas, R., "Mechanical Engineering Design, McGraw Hill", 9th Edition, p 475

[6] D. Katherasan, P. Sathiya, A. Raja, "Shielding gas effects on flux cored arc welding of AISI 316L (N) austenitic stainless-steel joints". Materials and Design 45 (2013) 43–51

[7] Adak D.K., Mukherjee M., Pal T., "Development of a Direct Correlation of Bead Geometry, Grain Size and HAZ Width with the GMAW Process Parameters on Bead-on-plate Welds of Mild Steel". Transactions of the Indian Institute of Metals, 68(5),(2015) 839-849.

Authors: **Varun Gupta, Student, Vinayak Mehra, Student, Pradeep Khanna, Associate Prof.**, Division of MPAE, Netaji Subhas University of Technology, New Delhi-110078, India.

E-mail: varungupta515@gmail.com
vinayak.mehra@gmail.com
4.khanna@gmail.com